# Crystal Structure of C-T-C-T-C-G-A-G-A-G. Implications for the Structure of the Holliday Junction[†,‡]

David S. Goodsell,[§] Kazimierz Grzeskowiak, and Richard E. Dickerson*

*Molecular Biology Institute, Department of Chemistry and Biochemistry & Institute of Geophysics and Planetary Physics, University of California, Los Angeles, California 90024*

*Received August 4, 1994; Revised Manuscript Received October 28, 1994*[⊗]

ABSTRACT: The structure of the B-DNA decamer of sequence C-T-C-T-C-G-A-G-A-G shows a crossed arrangement of helices in the *C*2 crystal lattice. This is the fourth example of a crossed arrangement of B-DNA oligomers in a crystal, and in spite of the fact that each of these four crystallizes in a different lattice, all have nearly identical structures at the crossing contact. This ubiquitous crossing arrangement may be used to generate a structure for the Holliday junction that is fully consistent with the available physical data.

Genetic recombination is thought to proceed through a four-armed, Holliday junction intermediate. The junction and its resolution by nucleophilic cleavage were first proposed by Holliday (1964). Physical studies on model junctions (Eis & Millar, 1993; Clegg et al., 1992; Murchie et al., 1989; Churchill et al., 1988; Duckett et al., 1988; Cooper et al., 1987) have determined several structural features of the intermediate: (1) base stacking is uninterrupted, forming two pseudocontinuous helices; (2) a right-handed, antiparallel arrangement of the two helices is preferred; (3) the helices are oriented at an acute angle relative to one another; (4) the strands exchange to form an uncrossed structure; and (5) divalent cations are necessary to form a stable structure. In addition, the cleavage sites for several resolving enzymes are known to a resolution of one base relative to the crossover point.

Two similar stacked-X models for the junction have been proposed, both of which are consistent with the preceding data. The first has been presented by Lilley and co-workers in conjunction with extensive biochemical analyses of model junctions and resolving enzymes (Murchie et al., 1989). Two DNA helices are placed side-by-side in an antiparallel orientation and are then brought together until phosphates from each helix just touch. Strand exchange is made at this one closest point of contact [see Figure 3 of Murchie et al. (1989) and Figure 8 of this work]. Sterically reasonable computer models of this junction have been built by Bhattacharyya et al. (1991) and by von Kitzing et al. (1990).

A second family of models has been presented by Timsit and Moras (1991, 1994). Two helices are aligned like those found in the crystal structure of A-C-C-G-G-C-G-C-C-A-

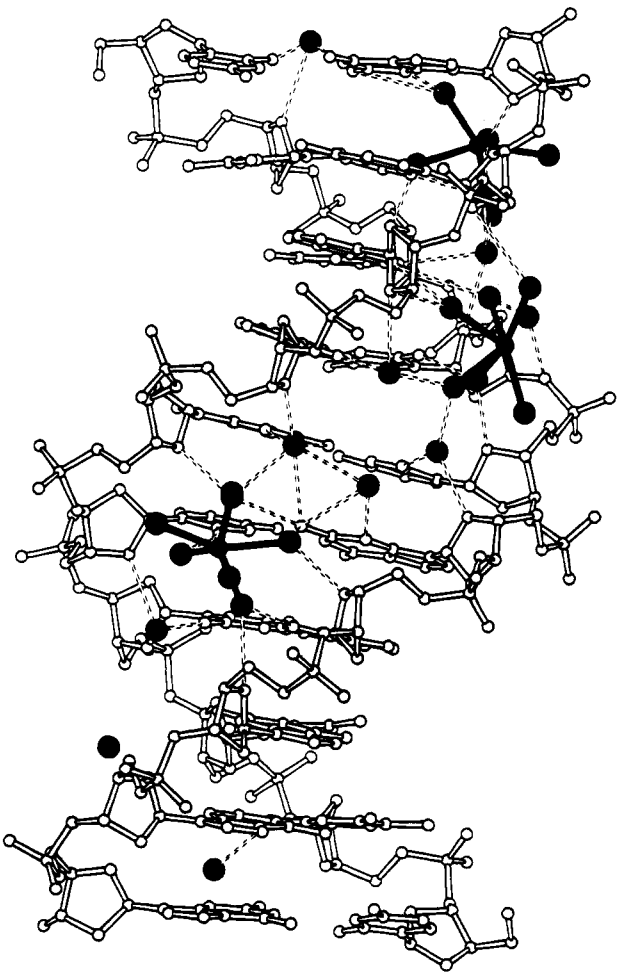

FIGURE 1: Structure of C-T-C-T-C-G-A-G-A-G. The decamer C-T-C-T-C-G-A-G-A-G adopts a typical B-helical form in the *C*2 crystal. Base pair C1·G20 is at the top of the helix, and C11·G10 is at the bottom. Although the base sequence is self-complementary, the two ends of the decamer helix are crystallographically independent. The water structure in the minor groove is shown, with the water molecules indicated by black spheres and distances of less than 3.5 Å marked by dotted bonds. Three calcium ions are located in the minor groove, shown as smaller black spheres connected to their hydration spheres by filled bonds.

[†] This work was performed with the support of NSF Grant MCB-8916261.

[‡] The experimental intensities and atomic coordinates have been deposited with the Brookhaven Protein Data Bank under file name 196D.

[§] Current address: Department of Molecular Biology, Scripps Research Institute, La Jolla, CA 92037.

[⊗] Abstract published in *Advance ACS Abstracts,* December 15, 1994.

0006-2960/95/0434-1022$09.00/0 

Table 1: Crossed-Helix Structures Discussed in This Paper

| space group | sequence | *a* (Å) | *b* (Å) | *c* (Å) | $\beta$ (deg) | helix crossing angle (deg) | reference |
|---|---|---|---|---|---|---|---|
| (a) *R*3 | A-C-C-G-G-C-G-C-C-A-C-A and variants | 67.0 | 67.0 | 48.0 | 120 | 74 | Timsit et al., 1989, 1991 |
| (b) *R*3 | C-C-G-G-C-G-C-C-G-G | 54.07 | 54.07 | 44.59 | 120 | 77 | Heinemann et al., 1992 |
| (c) $P3_221$ | C-G-A-T-C-G-$^{6me}$A-T-C-G | 33.38 | 33.38 | 98.30 | 120 | 60 | Baikalov et al., 1993 |
| | C-C-A-A-I-T-T-G-G | 33.23 | 33.23 | 94.77 | 120 | 60 | Lipanov et al., 1993 |
| | C-C-A-C-T-A-G-T-G-G | 32.9 | 32.9 | 95.1 | 120 | 60 | Shakked et al., 1994 |
| | C-C-A-T-T-A-A-T-G-G | 33.20 | 33.20 | 96.04 | 120 | 60 | Goodsell et al., 1994 |
| (d) *C*2 | C-T-C-T-C-G-A-G-A-G | 62.23 | 24.32 | 40.83 | 126.8 | 43 | this work |

Table 2: Root-Mean-Square Deviations of the Final Structure from Ideal Geometry and Standard Deviations

| | rms | $\sigma$ |
|---|---|---|
| Positional Constraints | | |
| bonds | 0.021 | 0.025 |
| distance across angles | 0.036 | 0.035 |
| phosphate bonds | 0.037 | 0.025 |
| distance across phosphate angles | 0.045 | 0.035 |
| planes | 0.021 | 0.020 |
| chiral centers | 0.166 | 0.150 |
| single-torsion contacts | 0.087 | 0.100 |
| multiple-torsion contacts | 0.103 | 0.100 |
| Isotropic Thermal Constraints | | |
| across bonds | 3.632 | 6.000 |
| across angles | 4.141 | 6.000 |
| across phosphate bonds | 4.587 | 6.000 |
| across phosphate angles | 5.106 | 6.000 |

C-A (Table 1, row a), and strands are exchanged at regions of close contact. Helices pack at an angle of 74° to one another in the crystal lattice, allowing phosphate backbones to interdigitate and form direct contacts between the phosphates on one helix and the base edges on a neighbor. Reasonable geometries were obtained by computer modeling for three different strand exchange sites, with several different chain topologies (these will be discussed in full later). The models are consistent with the physical data, but their geometry of interaction with resolving enzymes was not addressed in the Timsit–Moras papers. Recently, two additional families of crossed-helix packing arrangements in B-DNA crystals have been reported, as listed in Table 1, rows b and c. The four trigonal structures listed under Table 1 (row c) are mutually isomorphous. But the two rhombohedral structures in Table 1 (rows a and b) are not isomorphous; they have different unit cell dimensions, different molecular size (dodecamer vs decamer), and different crystal packing interactions.

In this report, we describe the structure and packing of the DNA oligomer C-T-C-T-C-G-A-G-A-G, which provides a fourth example of a crossed packing arrangement in B-DNA crystals (Table 1, row d). Although the crystal lattices in all four families of Table 1 are entirely different, the structures of the crossing contacts are virtually identical. We will generalize the modeling results of Timsit and Moras to describe how this ubiquitous crossing arrangement can yield a model of the Holliday junction that is fully consistent with the available data.

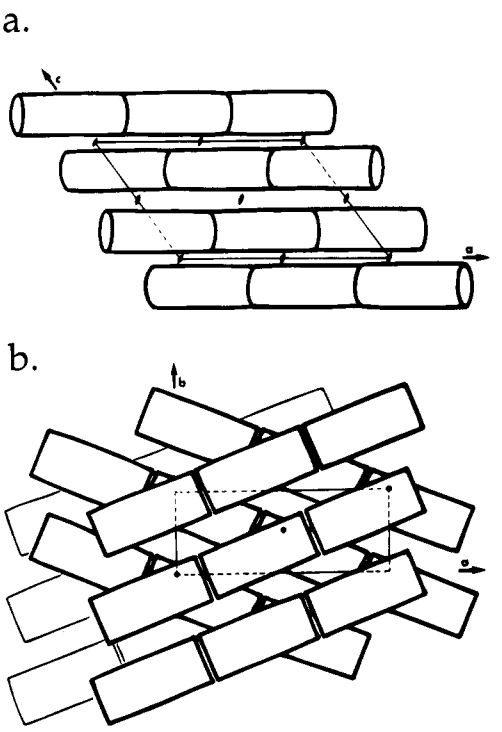


FIGURE 2: Crystal packing of C-T-C-T-C-G-A-G-A-G. Individual decamer double helices are drawn as cylinders with two-thirds the proper radius in the new *C*2 lattice. In the view down the crystallographic *b*-axis (a), layers of helices are viewed edge-on. The view 90° away (b), viewing the *ab* plane face-on, shows the crossing interaction between stacked layers. Dots mark lattice positions (0, 0, 0), ($^1/_2$, $^1/_2$, 0), and (1, 1, 0). The lower two layers in panel a correspond to the front two layers in panel b.

## MATERIALS AND METHODS

The DNA decamer C-T-C-T-C-G-A-G-A-G was synthesized by solid-phase phosphoramidite chemistry. Crystals were grown from standing drops at 5 °C from a solution of 1.34 mM DNA duplex, 100–250 mM calcium acetate, and 15–19% (v/v) 2-methyl-2,4-pentanediol (MPD). Large monoclinic prisms were obtained after equilibration against a reservoir of 60% (v/v) MPD. Data were collected with an R-AXIS-II imaging plate detector at −180 °C. One crystal yielded 4946 reflections with $R_{merge} = 5.6\%$, and 87% complete to 1.7 Å resolution. The overall *B* from a Wilson plot is 16%. The space group is *C*2, with $a = 62.23$ Å, $b = 24.32$ Å, $c = 40.83$ Å, $\beta = 126.78°$, and one decamer double helix per asymmetric unit.

The structure was solved by molecular replacement in XPLOR (Brunger et al., 1987), using data from 8.0 to 3.2 Å resolution. An ideal B-DNA helix of the proper sequence (Chandrasekaran & Arnott, 1989) yielded a clear solution,

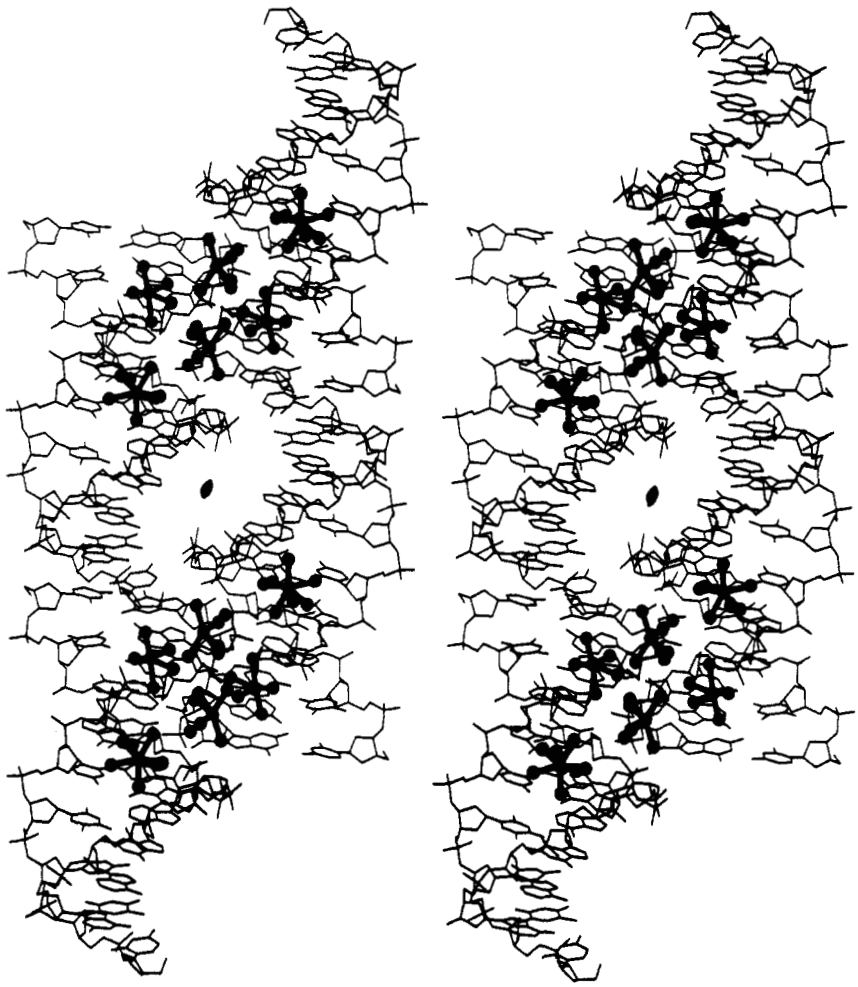

FIGURE 3: Calcium ions at the helix crossing contact. Four decamers are viewed down the *b*-axis at the 2-fold axis contact. The symmetry axis at the center corresponds to the lower central one in Figure 2a. Three crystallographically unique hydrated calcium ions (balls-and-sticks) mediate the close contact between helices. The full crossed-helix contact involves four individual decamers, yielding, by symmetry, the 12 calcium ions seen here.

after a rotation search followed by Patterson correlation refinement. A translation search using this orientation gave one clear solution. Rigid body refinement of this solution progressively using 1, 2, 4, 10, and 20 articulated groups yielded a model with $R$ = 37.3% to 3.2 Å resolution. Positional refinement with NUCLSQ (Hendrickson & Konnert, 1980) lowered this to $R$ = 34.8%. Data were added in 12 equal volume shells to 2.0 Å resolution, yielding $R$ = 33.4% but falling to $R$ = 31.7% after $B$-value refinement. Maps were calculated at this point. Thirteen water positions were added to strong density sites, and then data were added in 12 equal volume shells to 1.7 Å resolution, with $R$ = 29.4%. Solvent positions were assigned in groups of 10–15, with positional and $B$-value refinement after each set. Six water positions were assigned as calciums on the basis of (1) a proper water coordination sphere and (2) either excess $F_o - F_c$ density or an unusually low $B$-value. The final model contains 404 DNA atoms, 114 water positions, and 6 calcium ions, with $R$ = 18.3% using 4946 reflections greater than $2\sigma(F)$ to 1.7 Å resolution. Statistics for the refinement are included in Table 2. Both the experimental intensities and the atomic coordinates have been deposited with the Brookhaven Protein Data Bank for immediate distribution.

## RESULTS AND DISCUSSION

*Structure and Crystal Packing of C-T-C-T-C-G-A-G-A-G.* C-T-C-T-C-G-A-G-A-G adopts a nearly ideal B-helical structure in this new $C2$ crystal lattice (Figure 1). The helix shows an average twist angle of 35.5°, or 10.14 base pairs per turn. The minor groove is consistently wide, with a typical well-ordered double spine of hydration. Three fully hydrated calcium ions sit in the minor groove, with some of their coordinating waters contributing to the local hydration ribbons. The major deviation from ideality is a substantial tilt of the bases at the T4-C5 step, which may be explained by an invasive crystal contact at this point. Full details of the local structure and hydration of C-T-C-T-C-G-A-G-A-G will be presented in a later report, in conjunction with a study of the sister sequence, C-T-C-A-G-C-T-G-A-G, now in progress.

The packing of helices into the $C2$ cell is perhaps the most interesting aspect of the structure (Figure 2). As with almost all other crystals of B-DNA decamers, helices stack end-to-end to form a pseudocontinuous helical rod, with typical

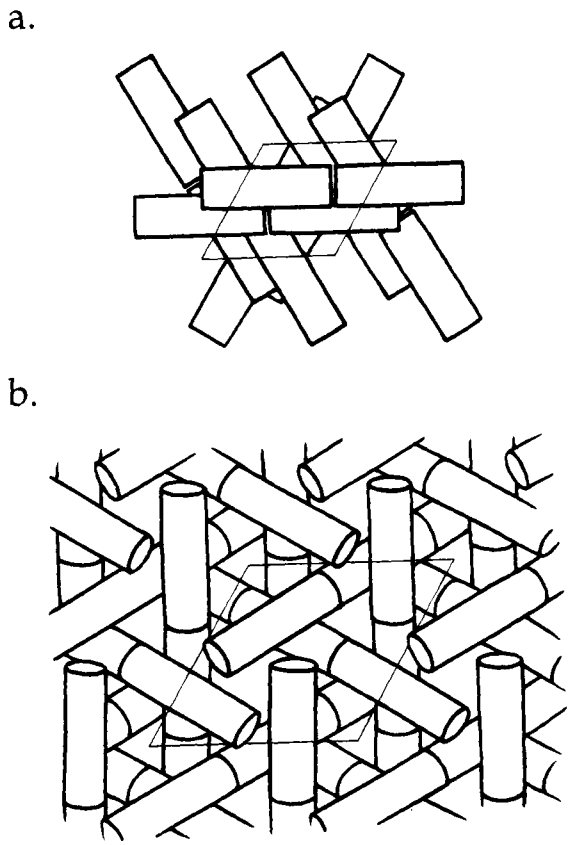


FIGURE 4: Crystal packing in trigonal and rhombohedral space groups. Schematic diagrams of helix packing in the $P3_221$ (a) and $R3$ (b) lattices, drawn in the style of Figure 2. In each case, the view is down the crystallographic $c$-axis, with the $ab$ plane in the plane of the page.

base−base stacking interactions at the junction. These pseudocontinuous helices then interact side-by-side to form a layer of helices along the face diagonal of the $ab$ plane. Helices at the (0, 0, 0) position and the ($^1/_2$, $^1/_2$, 0) position along this diagonal rod produce the $c$ centering shown in Figure 2b. These layers then are stacked along $c$ to build up the complete crystal (Figure 2a).

Adjacent layers in Figure 2a are related by 2-fold axes along $b$. An unusually intimate interaction is formed between individual helices in the top two layers and the bottom two layers of Figure 2a, interdigitating the backbones of the two helices and forming an angle of 42.5° between helix axes. The contact is mediated by a cluster of hydrated calcium ions, which bind in the minor groove on either side of a close approach with a neighboring phosphate group (Figure 3). Contacts between the second and third layers, across the middle of the cell at $c = {}^1/_2$, are less extensive.

*A Ubiquitous Crossed-Helix Interaction.* The packing of C-T-C-T-C-G-A-G-A-G in the $C2$ cell is the fourth independent example of crossed-helix packing in DNA oligomers. As listed in Table 1, the other three examples are the two quite different dodecamer and decamer structures in space group $R3$ and the family of isomorphous decamers in space group $P3_221$. Crystal packing in this latter family is shown in Figure 4a, and packing in the $R3$ rhombohedral decamer C-C-G-G-C-G-C-C-G-G is compared in Figure 4b. All other B-DNA crystal structures reported to date have contained

Table 3: Junction Distances in Four Crystal Lattices[a]

| junction | $C2$ | $P3_221$ | $R3$ (dodecamer)[b] | $R3$ (decamer)[b] |
|---|---|---|---|---|
| type A | 11.6 | 10.5 | 8.4 | 8.9 |
| type B | 4.8 | 5.8 | 7.8, 8.8 | 5.9, 5.9 |
| type C | 4.6 | 4.4 | 7.7, 8.2 | 7.3, 7.9 |
| type D | 6.4 | 11.1 | 14.0, − | 14.1, 15.1 |

[a] The shortest O3′−O5′ distance for each type of contact is given in angstroms. Distances were measured in an interactive computer graphics session. Type A junctions in the $C2$ and $P3_221$ lattices were measured between identical residues related by 2-fold symmetry. $C2$, C-T-C-T-C-G-A-G-A-G; $P3_221$, C-C-A-A-C-I-T-T-G-G; $R3$ (dodecamer), A-C-C-G-G-C-G-C-C-A-C-A; $R3$ (decamer), C-C-G-G-C-G-C-C-G-G. [b] In the $R3$ lattices, the two sides of the crossing contact are crystallographically independent, so individual distances are given for B and B′, C and C′, and D and D′. Because of the unusual nature of the end-to-end helix stacking in the $R3$ dodecamer, one type D distance was not measurable.

only stacked helices packed side-by-side and parallel. The four families of Table 1 are the only examples of crossed, nonparallel packing arrangements in B-helical DNA oligomers, and the present decamer is the first interlocking groove structure to pack into a cell without a trigonal axis.

Although the arrangements of helices in these four lattices are quite different, the interlocking crossing contacts of helices are virtually identical. Backbones interdigitate such that phosphates make contact with bases in the major groove (Figure 5). A 2-fold or pseudo-2-fold axis bisects the obtuse angle, relating the walls of the major groove of each helix to one another (Figure 6). Crossing angles range from 42.5° to 77.1°, depending on the space group. The different angles in the four structures are accommodated by small variations in distance between the helices.

According to the conventions of Lilley and co-workers (Murchie et al., 1989), the two helices in the $C2$ and $P3_221$ packing arrangements are in a right-handed orientation, with identical sequences antiparallel. That is, the upper helix is superimposable onto the lower by a right-handed rotation that closes the acute angle between them (43° in Figure 6a or 60° in Figure 6b), and when this is done, equivalent chains in the two helices are observed to be traveling in opposite directions. Of course, this is an inevitable consequence of the 2-fold axis through the obtuse angle relating one helix to the other. In the two different $R3$ packing arrangements (Figure 6c,d), the two helices are also in a right-handed orientation, but since the local sequences are not related by a 2-fold symmetry axis, nonhomologous sequences interact at the contact, so that the terminology of parallel vs antiparallel is ambiguous and not useful.

*Models of the Holliday Junction.* Several models of the Holliday intermediate may be generated starting from the packing arrangement observed in these structures. In four places, the helices come close enough together that strand exchange is possible, and these are identified as junction sites A−D in the upper part of Figure 7. For each of the experimental crystal structures, the closest distance from O3′ in one helix to O5′ in a neighbor for each type of junction is listed in Table 3. Site A sits on the dyad axis; the other three possible exchange sites are repeated in pairs across the

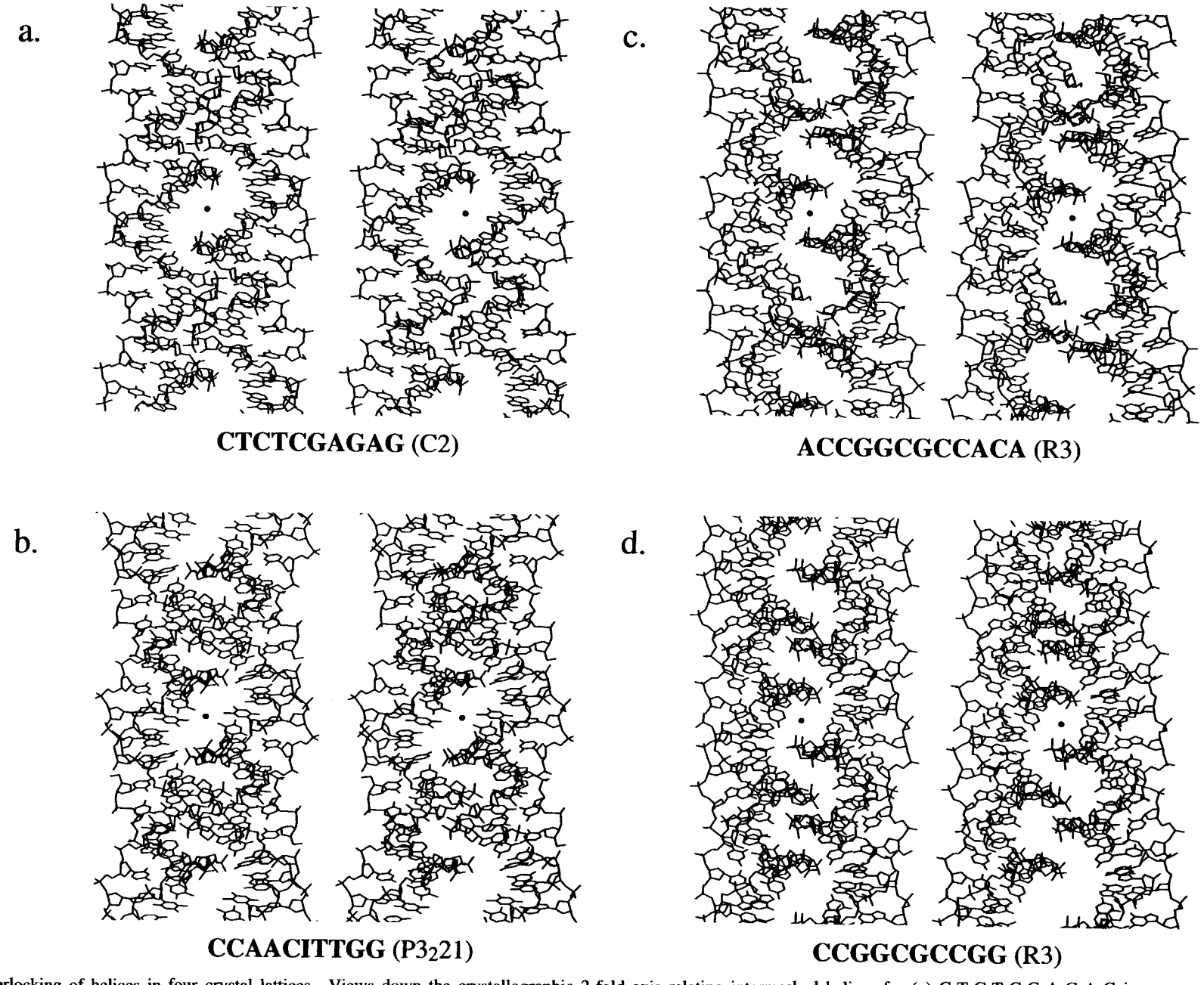


FIGURE 5: Interlocking of helices in four crystal lattices. Views down the crystallographic 2-fold axis relating intermeshed helices for (a) C-T-C-T-C-G-A-G-A-G in space group *C*2 and (b) C-C-A-A-C-I-T-T-G-G in space group $P3_221$. Equivalent views down the pseudo-2-fold axes in space group *R*3 for (c) A-C-C-G-G-C-G-C-C-A-C-A and (d) C-C-G-G-C-G-C-C-G-G.

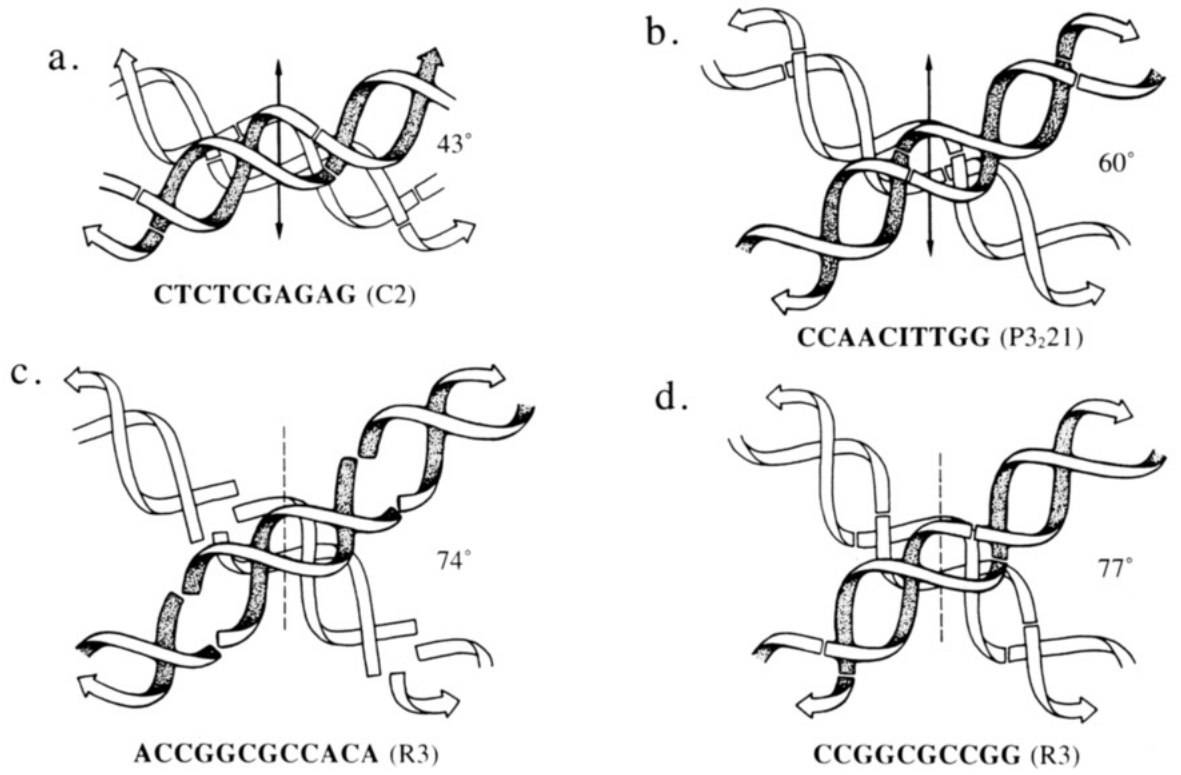


FIGURE 6: Crossing arrangement in four crystal lattices. Schematic helical ribbon drawings, prepared from actual coordinates, of the four helix crossings of Figure 5, but this time with the 2-fold axis (black arrow) or pseudo-2-fold axis (dotted line) vertical in the plane of the page. The angle of crossing is given next to each diagram. Arrows on the backbone ribbons indicate the 5′-to-3′ direction. Breaks between individual helices are drawn on each ribbon. Note that the end-on-end stacking of helices is more regular in the decamers (a, b, d) than in the dodecamer (c), which contains 1.2 helical turns per molecule.

2-fold axis: B and B′, C and C′, and D and D′.

If, after strand exchange, each strand continues on in its original direction (left or right in Figure 7), the strands are said to be crossed; if a strand doubles back to follow the direction from which it came, it is said to be uncrossed. This terminology arises from the point of view that the left ends of the two helices in Figure 7 are in some sense equivalent ends, as though the acute angle were to be closed down to zero. If, in contrast, one were to open up the acute angle to 180° and close down the obtuse angle to zero, then the lower left and lower right helix ends in Figure 7 would be associated, and the meanings of crossed and uncrossed would be reversed. To preserve the proper 5′-to-3′ sense after a strand exchange, sites A and C form noncrossed junctions in the sense just described, and B and D form crossed junctions.

Two strand-exchange topologies are possible at each of the four possible sites: strands may reverse directions in an unlinked manner (as in the main drawings of Figure 7) or they may link "elbows" (as in the small insets of Figure 7). Hence, eight different single-site strand-exchange models are possible: A−D, all either linked or unlinked. Note that if one of the helices is rotated end-for-end in Figure 7, a linked structure becomes unlinked and vice versa. This end-for-end rotation also changes crossed junctions to uncrossed and parallel junctions to antiparallel.

Four of these eight fundamental strand exchanges have been modeled previously, on the basis of the rhombohedral

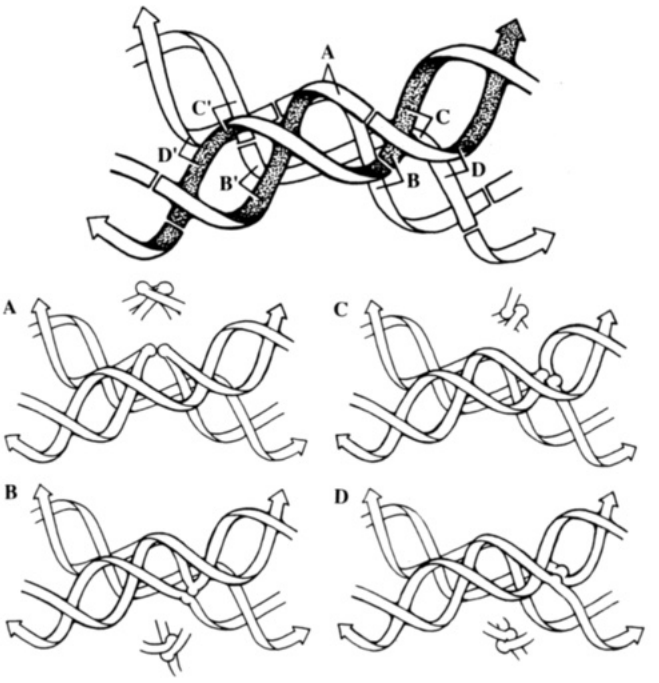


FIGURE 7: Models of the Holliday junction. Four unique close contacts between helices are observed in the crossing arrangement of C-T-C-T-C-G-A-G-A-G, labeled A−D. Strand exchange at each site yields uncrossed junctions at A and C and crossed junctions at B and D. The closest O3′−O5′ distances at each contact, for each of the four different crossing angles shown in Figure 4, are given in Table 3. Note that type B, C, and D strand exchanges can be performed to either the right or left of the 2-fold symmetry axis (B vs B′, etc.). Only one type A strand exchange is possible because that site sits on the 2-fold symmetry axis.

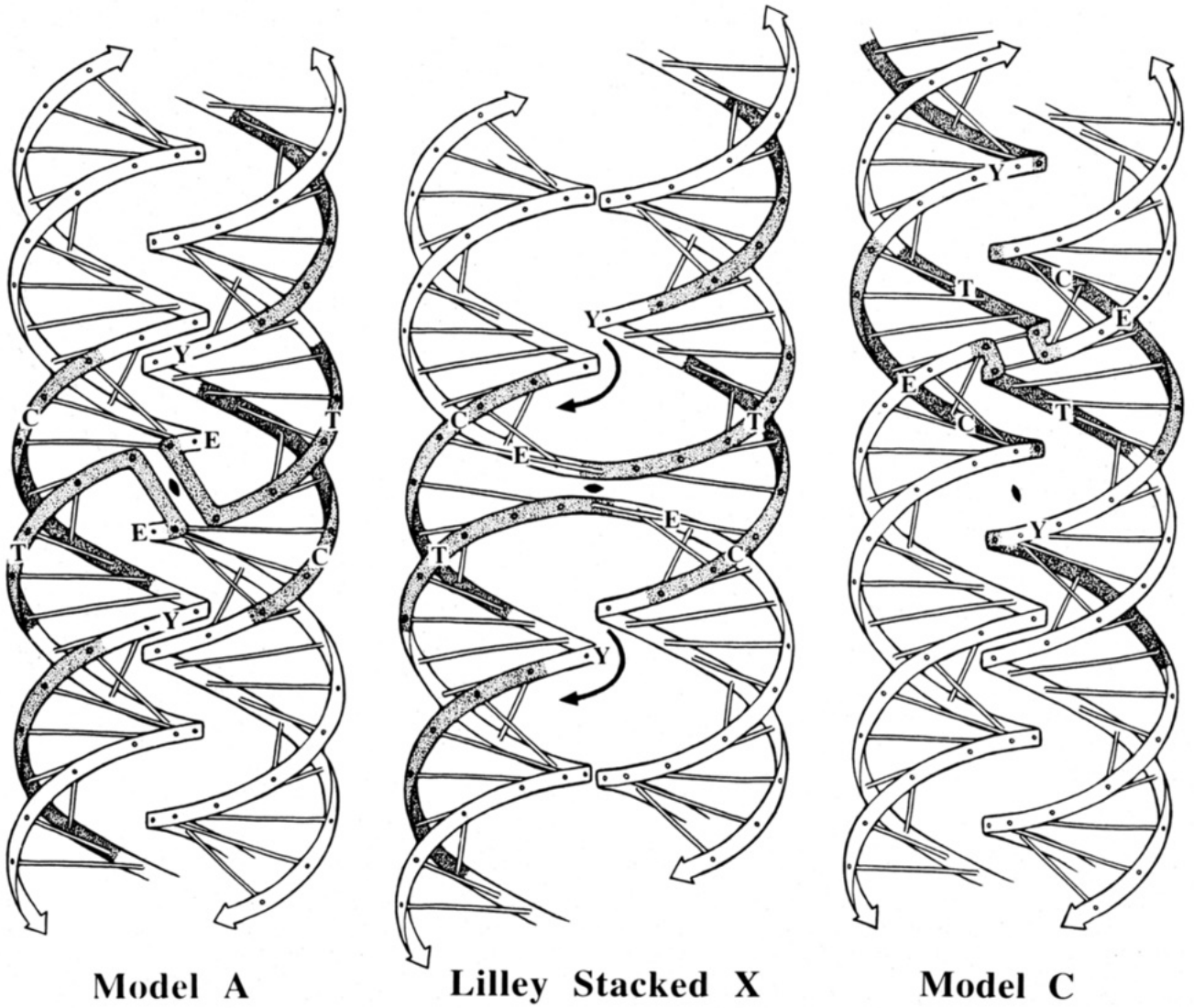


FIGURE 8: Evaluation of models. The sites of cleavage of yeast (Y), calf (C), T4 (T), and *E. coli* (E) resolving enzymes are mapped onto type A and type C junctions and onto the stacked-X model proposed by Lilley and co-workers (Murchie et al., 1989). Regions that are protected by T4 endonuclease VII in footprinting experiments are shaded in each diagram. Both the type A and Lilley junctions place the cleavage sites on one face of the junction and show typical geometry expected for the enzyme footprint. The asymmetrical type C junction is inconsistent with these data, placing the cleavage sites and footprint on both sides and through the middle of the junction. The model of Lilley may be converted to model A by a shift in registration (arrows), so that the phosphate backbones of one helix fit snugly into the grooves of the other.

packing of A-C-C-G-G-C-G-C-C-A-C-A (Timsit & Moras, 1991): type C unlinked, type B unlinked, and type A linked and unlinked. (The nomenclature of Timsit and Moras has been modified to reflect the location of each exchange site relative to the 2-fold axis of symmetry—our types A, B, and C are their III, II, and I, respectively.) Sterically reasonable structures were obtained in each case. In addition, a double strand exchange in the type C junction was modeled, with crossovers at both C and C′ in Figure 7. Note that a double crossover is possible at any of the three asymmetrical sites—B, C, and D—and each of the two sites in each double exchange may yield either a linked or an unlinked junction.

Unlinked models A and C fit all of the criteria imposed by the physical experiments mentioned earlier: they are composed of two pseudocontinuous helices in a right-handed antiparallel orientation, with an uncrossed junction (B and D are crossed). The location of calcium ions in the structure of C-T-C-T-C-G-A-G-A-G is consistent with the observed requirement for divalent cations in the formation of Holliday junctions (Duckett et al., 1990); such cations are necessary to mediate the close approach of negatively charged phosphates.

Mapping of cleavage sites of calf, yeast, T4, and *Escherichia coli* resolving enzymes and the footprint of T4 endo VII [*E. coli* from Bennett et al. (1993); others from Bhattacharyya et al. (1991)] reveals a clear preference for model A over model C (Figure 8). Model A places all four sites of cleavage on one side of the junction, and the footprint protection regions are consistent with contacts that one might expect from the approach of a compact dimeric enzyme. In contrast, model C places the yeast cleavage site on the side of the helix opposite the T4 and calf sites and smears the enzyme footprint protection zone onto both the front and the back and through the middle of the junction itself. Model A also is favored due to its 2-fold symmetry axis through the junction, consistent with the putative 2-fold symmetry

of dimeric resolving enzymes.

Comparison of model A with that proposed by Lilley and co-workers (Murchie et al., 1989) shows that both models account equally well for the cleavage sites and footprint data (Figure 8). The two models are topologically similar, although different in many details. The Lilley model may be transformed into model A by counterrotating the two helices by roughly one-eighth turn, bringing the junction slightly toward the front and shifting the registration of helices by about 3 base steps, as shown by the curved arrows in Figure 8. [See also Figure 16 of Baikalov et al. (1993) for a view of the transition 90° to the left of that of Figure 8.]

The advantage of model A over the Lilley model is that it readily explains the preference for right-handed crossing and the observed rigidity of the stacked-X structure. The interlocking of phosphate backbones into grooves (Figure 3) demands a right-handed crossing, as measured relative to the acute crossing angle. One might expect that the looser model of Lilley, with its simple cylinder contacts, would not exhibit a significant orientational preference for right- vs left-handed crossing.

The recent crystal structure analysis of *E. coli* RuvC protein (Ariyoshi et al., 1994) provides the first atomic look at a protein that acts on a Holliday intermediate. Modeling of a proposed DNA structure, based on the coordinates of the protein alone, resulted in a structure having two base pairs of each helix melted, but with more or less continuous side-by-side helices. As noted by the authors, this model significantly differs from the stacked-X models of Lilley and model A as presented here. However, analysis of hydroxyl radical hypersensitivity of the RuvC junction complex (Bennett et al., 1993) has been interpreted to suggest that a significant distortion of the DNA occurs upon binding. Thus, the stacked-X models may be valid for a Holliday intermediate in the absence of enzyme and during the initial recognition and binding step, if not for the enzyme-bound intermediate.

## REFERENCES


Ariyoshi, M., Vassylyev, D. G., Iwasaki, H., Nakamura, H., Shinagawa, H., & Morikawa, K. (1994) *Cell 78*, 1063−1072.

Baikalov, I., Grzeskowiak, K., Yanagi, K., Quintana, J., & Dickerson, R. E. (1993) *J. Mol. Biol. 231*, 768−784.

Bennett, R. J., Dunderdale, H. J., & West, S. C. (1993) *Cell 74*, 1021−1031.

Bhattacharyya, A., Murchie, A. I. H., von Kitzing, E., Diekmann, S., Kemper, B., & Lilley, D. M. J. (1991) *J. Mol. Biol. 221*, 1191−1207.

Brunger, A. T., Kuriyan, J., & Karplus, M. (1987) *Science 235*, 458−460.

Chandrasekaran, R., & Arnott, S. (1989) in *Landolt-Bornstein, New Series, Group VII* (Saenger, W., Ed.) Vol. 16, pp 130−170, Springer-Verlag, New York.

Churchill, M. E. A., Tullius, T. D., Kallenbach, N. R., & Seeman, N. C. (1988) *Proc. Natl. Acad. Sci. U.S.A. 85*, 4653−4656.

Clegg, R. M., Murchie, A. I. H., Zechel, A., Carlberg, C., Diekmann, S., & Lilley, D. M. J. (1992) *Biochemistry 31*, 4846−4856.

Cooper, J. P., & Hagerman, P. J. (1987) *J. Mol. Biol. 198*, 711−719.

Duckett, D. R., Murchie, A. I. H., Diekmann, S., von Kitzing, E., Kemper, B., & Lilley, D. M. J. (1988) *Cell 55*, 79−89.

Duckett, D. R., Murchie, A. I. H., & Lilley, D. M. J. (1990) *EMBO J. 9*, 583−590.

Eis, P. S., & Millar, D. P. (1993) *Biochemistry 32*, 13852−13860.

Goodsell, D. S., Kaczor-Grzeskowiak, M., & Dickerson, R. E. (1994) *J. Mol. Biol. 239*, 79−96.

Heinemann, U., Alings, C., & Bansal, M. (1992) *EMBO J. 11*, 1931−1939.

Hendrickson, W. A., & Konnert, J. H. (1980) in *Computing in Crystallography* (Diamond, R., Ramaseshan, S., & Venkatesan, K., Eds.) pp 13.01−13.23, Indian Academy of Sciences, Bangalore, India.

Holliday, R. (1964) *Genet. Res. 5*, 282−304.

Lipanov, A., Kopka, M. L., Kaczor-Grzeskowiak, M., Quintana, J., & Dickerson, R. E. (1993) *Biochemistry 32*, 1373−1389.

Murchie, A. I. H., Clegg, R. M., von Kitzing, E., Duckett, D. R., Diekmann, S., & Lilley, D. M. J. (1989) *Nature 341*, 763−766.

Shakked, Z., Guzikevich-Guerstein, G., Frolow, F., Rabinovich, D., Joachimiak, A., & Sigler, P. B. (1994) *Nature 368*, 469−473.

Timsit, Y., & Moras, D. J. (1991) *J. Mol. Biol. 221*, 919−940.

Timsit, Y., & Moras, D. J. (1994) *EMBO J. 13*, 2737−2746.

Timsit, Y., Westof, E., Fuchs, R. P. P., & Moras, D. (1989) *Nature 341*, 459−462.

Timsit, Y., Vilbois, E., & Moras, D. (1991) *Nature 354*, 167−170.

von Kitzing, E., Lilley, D. M. J., & Diekmann, S. (1990) *Nucleic Acids Res. 18*, 2671−2683.


BI941794V